Journal of Hazardous Materials 160 (2008) 70–77

Contents lists available at ScienceDirect

Journal of Hazardous Materials

journal homepage: www.elsevier.com/locate/jhazmat

Application of nanofiltration for the rejection of nickel ions from aqueous solutions and estimation of membrane transport parameters

Z.V.P. Murthy*, Latesh B. Chaudhari

Department of Chemical Engineering, S.V. National Institute of Technology, Surat 395007, Gujarat, India

ARTICLE INFO

Article history:
Received 26 May 2007
Received in revised form
23 September 2007
Accepted 26 February 2008
Available online 4 March 2008

Keywords:
Membrane transport model
Concentration polarization modulus
Peclet number

ABSTRACT

The present work deals with the application of a thin-film composite polyamide nanofiltration membrane for the rejection of nickel ions from aqueous wastewater. The operating variables studied are feed concentration (5–250 ppm), applied pressure (4–20 atm), feed flowrate (5–15 L/min) and pH (2–8). It is observed that the observed rejection of nickel ions increases with increase in feed pressure and decreases with increase in feed concentration at constant feed flowrate. The maximum observed rejection of the metal is found to be 98% and 92% for an initial feed concentration of 5 and 250 ppm, respectively. The effect of pH on the rejection of nickel ions and permeate flux are studied, and found that the variation in pH is having more effect on the latter than the former. The experimental data are analyzed using membrane transport models; combined-film theory-solution-diffusion (CFSD), combined-film theory-Spiegler–Kedem (CFSK) and combined-film theory-finely porous (CFFP) models; to estimate membrane transport parameters and mass transfer coefficient, *k*. Also, enrichment factor, concentration polarization modulus and Peclet number are found from various parameters. From CFFP model the effective membrane thickness and active skin layer thickness are found.

1. Introduction

Wastewaters containing heavy metals are discharged to the environment by several industries, such as mining, metallurgical, electronic, electroplating and metal finishing. The removal of heavy metals from wastewaters is of critical importance due to their high toxicity and tendency to accumulate in living organisms. Moreover, heavy metals cannot be degraded or destroyed. Membrane separation processes with different types of membranes show great promise for commercial application [1,2]. Nanofiltration (NF) is the intermediate process between reverse osmosis (RO) and ultrafiltration (UF). NF is a promising technology for the rejection of heavy metal ions like nickel [3–5], cadmium [6,7], chromium [8], copper [9–11], and arsenic [12] from wastewater. NF process benefits from ease of operation, reliability and comparatively low energy consumption as well as high efficiency of pollutant removal [13–15]. Solute rejection in NF membrane involves mainly electrostatic interaction of membrane and solutes on the membrane surface and size exclusion [16]. Numerous models were used/proposed to describe and predict solute rejection/flux by NF based on extended Nernst–Planck equation [17]. The membrane properties were determined based on the charged and uncharged solute permeation test and the hypothetical mechanistic structure (pore size, effective thickness/porosity, and fixed charged density) was determined using Donnan steric pore-flow (DSP) model [18]. Straatsma et al. [19] developed an NF model based on the Maxwell–Stefan transport equations. The DSP model is used to predict permeate flux and rejection of multicomponent liquid feeds as a function of membrane properties (mean pore size, porosity, thickness, and surface-charge characteristics) and applied feed pressure. These models are mathematically complex, computationally expensive and they ideally require a very detailed knowledge of the filtration process as well as characterization of the membrane [20]. Therefore, there is a need to find an alternative means for predicting process performance by exploiting available process data and extending it to unavailable data. Spiegler–Kedem model and solution-diffusion model are capable of modelling highly complex and nonlinear systems for NF membranes. Spiegler–Kedem model [21–24] treats membrane cell as a black box and characterizes it in terms of salt permeability, P_M, and reflection coefficient, σ. Murthy and Gupta [25] suggested that the combined-film theory-Spiegler–Kedem (CFSK) model may be the better method for estimation of membrane transport parameters and mass transfer coefficient, simultaneously, for a given membrane cell of reverse osmosis, and which may also be applicable to nanofiltration.

* Corresponding author. Tel.: +91 261 2201641/2223371–4; fax: +91 261 2227334/2201641.
E-mail addresses: zvpm2000@yahoo.com, zvpm@ched.svnit.ac.in (Z.V.P. Murthy).

0304-3894/$ – see front matter © 2008 Elsevier B.V. All rights reserved.
doi:10.1016/j.jhazmat.2008.02.085

Nomenclature

a	constant in Eq. (24)
a_1	$\sigma/(1-\sigma)$
a_2	$(1-\sigma)/P_M$
A	proportionality constant in Eq. (5) (mol/cm^2 atm)
b	constant in Eq. (24)
b_c	channel height (cm)
b_f	friction factor in finely porous model
b_1	$(b_f\varepsilon/K)-1$
b_2	$\tau\delta/(\varepsilon D_{AB})$
c	constant in Eq. (24)
C_{Ai}	concentration of A at any position i (ppm)
$D_{AM}K/\delta$	solute transport parameter (cm/s)
D_{AB}	diffusivity of solute A in solvent B (cm^2/s)
D_{AM}	diffusivity of solute A in membrane (cm^2/s)
E_o	enrichment factor defined as C_{A3}/C_{A1}
E	enrichment factor in the absence of boundary layer defined as C_{A3}/C_{A2}
F	factor in Eq. (11)
J_v	solvent volume flux (cm/s)
k	mass transfer coefficient (cm/s)
K	solute partition coefficient
l	thickness of the concentration boundary layer (cm)
L	channel length (cm)
L_P	hydraulic permeability coefficient (cm/s atm)
Δp	pressure difference across the membrane (atm)
P_M	overall permeability coefficient (cm/s)
Q	feed flowrate (mL/min)
R	true rejection
Re	Reynolds number
R_o	observed rejection
Sc	Schmidt number
Sh	Sherwood number
U	linear circulation velocity (cm/s)

Greek letters

δ	effective thickness of a membrane (cm)
ε	void fraction of the membrane
$\Delta\pi$	osmotic pressure difference across the membrane (atm)
σ	reflection coefficient
τ	tortuosity of the membrane

Subscripts

A	solute
B	solvent
M	membrane
1	feed solution
2	boundary layer solution
3	permeate solution

The main aim of the present work is to investigate nickel ion removal from aqueous wastewater by a commercial NF-300 membrane by changing operating parameters; feed concentration, feed flowrate, pH and applied feed pressure. Also, the membrane transport parameters and mass transfer coefficient are found by using solution-diffusion, Spiegler–Kedem and finely porous models in combination with film theory model. In addition, the enrichment factors, concentration polarization modulus and Peclet number are estimated for the NF-300 membrane.

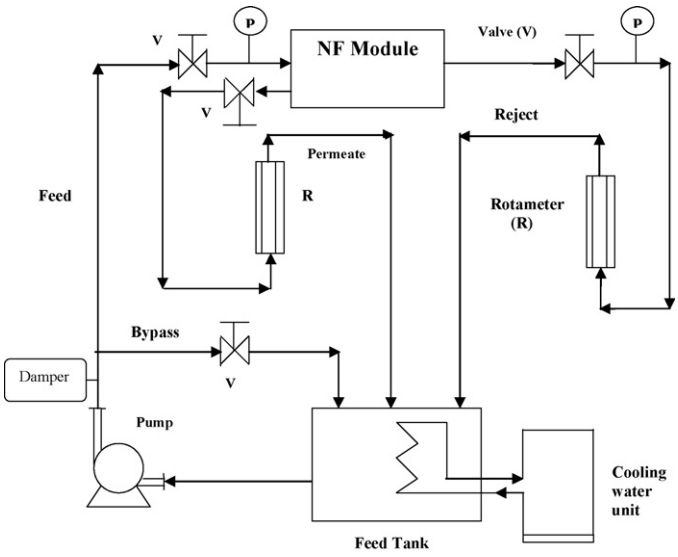

Fig. 1. Perma® pilot scale membrane system.

2. Materials and methods

Synthetic samples of wastewater are prepared by adding required amounts of nickel sulphate ($NiSO_4{\cdot}6H_2O$) to distilled water (pH 5.9 ± 0.2 and conductivity 1.0 μS/cm). Several solutions are prepared with different concentrations (5–250 ppm) of nickel sulphate. The experiments are performed on a Perma® pilot scale membrane system (Permionics, Vadodara, India). The experimental set-up is shown in Fig. 1. A rectangular flat membrane cell is used for the experiments. The membrane-housing cell, shown in Fig. 1, is made of stainless steel with two halves fastened together with high tensile bolts. The top half of cell contained the flow distribution chamber and the bottom half is used as the membrane support system. The membrane required support to prevent rupture at high hydrostatic pressures. The following arrangements of special supports are used: a perforated 1 mm thick stainless steel plate is laid over with a stainless steel gauge of 300 mesh size, which is topped by a Whatman filter paper and followed by the actual membrane with its active thin layer exposed to the high-pressure fluid. This arrangement provides sufficient mechanical support to the test membrane at high pressures. The upper half of the test cell contains a groove for the arrangement of HDPE 'O' ring to avoid leakage at high-pressure operation. Experiments are performed with a commercial thin-film composite polyamide membrane, Perma-TFC-NF-300 (Permionics, Vadodara, India), hereafter, referred as NF-300 membrane. This membrane has three layers. The first layer is a 5–20 μm polyamide polymer layer that does the actual rejection. The second layer is made of polysulfone of 50 μm thickness. The third layer, used to bear resistance and strength, is made of polyester with a thickness of about 150 μm. The Perma-TFC membranes are capable of withstanding pH in the range 2–12, pressure up to 30 atm and temperatures up to 50 °C. The NF-300 membrane is characterized by 300 Da cut-off. The effective membrane surface area is 150 cm^2. The 1 mm thin channel passage in the membrane test cell and the high cross-flow feed rates used in the experimentation will enable the system in controlling the concentration polarization. Before conducting the actual experiments for the rejection of nickel ions, the NF-300 membrane is subjected to stabilization at 20 atm, which is the maximum pressure used in the experiments, for 2 h to avoid possible membrane compaction during the experimentation. Experiments are performed for 2 h, for each set of rejection data, in batch circulation mode and the permeate samples are collected from high pressure to low pressure for

a particular feed concentration and feed flowrate. Both permeate and concentrate are returned to the feed vessel in order to keep constant feed concentration. Samples of permeate are collected at a given time interval, to measure the observed salt rejection (R_o) and permeate volume flux (J_v). The nickel ion concentrations are measured by an atomic absorption spectrophotometer (Model SL-173, M/S. ELICO Limited, Hyderabad, India) according to standard methods [26]. After each set of experiments for a given feed concentration, the set-up is rinsed with distilled water for 30 min at 4 atm to clean the system. This procedure is followed by measurement of pure water permeability (PWP) with distilled water to ensure that the initial membrane PWP is restored. The experiments are carried out for different feed concentrations (5, 50, 100, 150, 200 and 250 ppm), feed flowrates (5, 10 and 15 L/min), feed pressures (4, 8, 12, 16 and 20 atm), feed pH (2, 4, 6, 8 and 10) and the corresponding R_o and J_v are measured.

3. Membrane transport models

3.1. Film theory

The build up of solute concentration at the membrane–liquid interface during separation process is termed as concentration polarization. A material balance for the solute in a differential element, according to film theory and using relevant boundary conditions, will give [25]

$$\left(\frac{C_{A2}-C_{A3}}{C_{A1}-C_{A3}}\right)=\exp\left(\frac{J_v}{k}\right) \tag{1}$$

where the mass transfer coefficient, k, is equal to D_{AB}/l. All the notations are given in the nomenclature. Eq. (1) can be rearranged to give a relation between the observed rejection

$$R_o=\frac{C_{A1}-C_{A3}}{C_{A1}} \tag{2}$$

and the true rejection

$$R=\frac{C_{A2}-C_{A3}}{C_{A2}} \tag{3}$$

as

$$\frac{R_o}{1-R_o}=\left[\frac{R}{1-R}\right]\left[\exp\left(\frac{-J_v}{k}\right)\right] \tag{4}$$

The above Eq. (4) with an appropriate membrane transport model may now be used for determining the membrane parameters as well as mass transfer coefficient k.

3.2. Combined-film theory-solution-diffusion model

The working equations of the solution-diffusion model [27] are

$$J_v=A(\Delta p-\Delta\pi) \tag{5}$$

$$J_A=\left(\frac{D_{AM}K}{\delta}\right)(C_{A2}-C_{A3}) \tag{6}$$

where A is the permeability parameter of the solvent and can be estimated from pure water permeability measurements, and $(D_{AM}K/\delta)$ is considered as a single parameter, namely the solute transport parameter. Eqs. (5) and (6) may be combined with Eq. (3), as illustrated by Pusch [22], to give

$$\frac{1}{R}=1+\left(\frac{D_{AM}K}{\delta}\right)\left(\frac{1}{J_v}\right) \tag{7}$$

Eq. (7) predicts that R approaches 1.0 for infinite permeate flux. This is not realistic for many solutes, which do not approach perfect rejections at high permeate flux rates [28]. Eq. (7) can be rearranged to

$$\frac{R}{1-R}=\frac{J_v}{D_{AM}K/\delta} \tag{8}$$

Now, Eq. (8) can be substituted into Eq. (4) to give

$$\frac{R_o}{1-R_o}=\left[\frac{J_v}{D_{AM}K/\delta}\right]\left[\exp\left(-\frac{J_v}{k}\right)\right] \tag{9}$$

Eq. (9) is the present working equation of the combined-film theory-solution-diffusion (CFSD) model. By supplying R_o vs. J_v data, taken at different pressures but at a constant feed rate and constant feed concentration for each set, the parameter $(D_{AM}K/\delta)$ and the mass transfer coefficient, k, can be estimated numerically.

3.3. Combined-film theory-Spiegler–Kedem model

As reported in the literature [21], an irreversible thermodynamics (IT) model can be applied to explain the rejection performance of an uncharged solute and when there is no electrostatic interaction between membrane and solute. This is the case when the membrane is uncharged such as RO membrane or when the solute is neutral. Many authors [6,24] have extended this model in retention of electrolyte with an NF membrane that is charged. The working equations of the nonlinear Spiegler–Kedem model [21,22,25] are

$$J_v=L_P(\Delta p-\sigma\,\Delta\pi) \tag{10}$$

$$R=\frac{\sigma(1-F)}{1-\sigma F} \tag{11}$$

where

$$F=\exp\left[-J_v a_2\right] \tag{12}$$

with

$$a_2=\frac{1-\sigma}{P_M} \tag{13}$$

Here σ is the reflection coefficient which represents the rejection capability of a membrane, i.e., $\sigma=0$ means no rejection and $\sigma=1$ means 100% rejection, P_M is the overall permeability coefficient and L_P is the hydraulic permeability coefficient of the membrane, which is similar to A given in Eq. (5). Eq. (11) can be rearranged to give

$$\frac{R}{1-R}=a_1(1-F) \tag{14}$$

where

$$a_1=\frac{\sigma}{1-\sigma} \tag{15}$$

Now, substitution of Eq. (14) into Eq. (4) results in the following equation:

$$\frac{R_o}{1-R_o}=a_1[1-\exp(-J_v a_2)]\left[\exp\left(-\frac{J_v}{k}\right)\right] \tag{16}$$

Eq. (16) is the working equation for the combined-film theory-Spiegler–Kedem (CFSK) model. It may be noted that Eq. (16) reduces to Eq. (9) for σ value approaching 1. Once again, by using a nonlinear parameter estimation method by supplying the data of R_o vs. J_v taken at different pressures, but at constant feed rate and constant feed concentration for each set, we can estimate the membrane parameters σ and P_M and the mass transfer coefficient, k, simultaneously.

3.4. Combined-film theory-finely porous model

The working equation for finely porous model is [29,30]

$$\frac{1}{1-R}=\left(\frac{b_f\varepsilon}{K}\right)+\left(\frac{K-b_f\varepsilon}{K}\right)\exp\left(-J_v\frac{\tau\delta}{\varepsilon D_{AB}}\right) \tag{17}$$

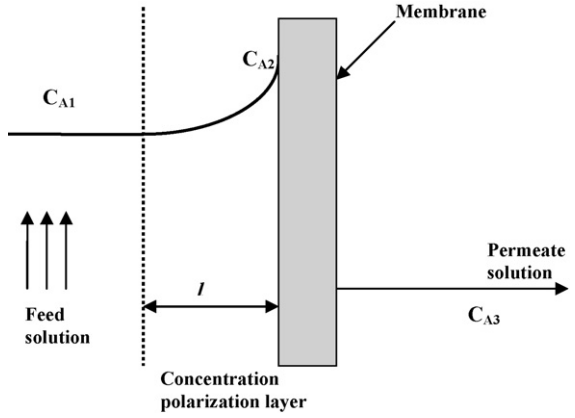

Fig. 2. Schematic of concentration profile on the solute in the feed and permeate solution near the membrane surface.

Using Eq. (4) with Eq. (17), one can get

$$\frac{R_o}{1-R_o} = \left(\frac{b_f \varepsilon}{K} - 1\right)\left[1 - \exp\left(-J_v \frac{\tau\delta}{\varepsilon D_{AB}}\right)\right] \exp\left(-\frac{J_v}{k}\right) \quad (18)$$

Here the parameters are

$$b_1 = \left(\frac{b_f \varepsilon}{K}\right) - 1 \quad (19)$$

$$b_2 = \frac{\tau\delta}{\varepsilon D_{AB}} \quad (20)$$

Eq. (18) is the combined-film theory-finely porous (CFFP) model. Using a nonlinear parameter estimation method, by supplying the data of R_o vs. J_v taken at different pressures but at constant feed rate and constant feed concentration for each set, one can estimate the membrane parameters and k, simultaneously.

3.5. Enrichment factors and concentration polarization modulus

As mentioned in Section 3.1, the concentration polarization is typically described via film theory model whereby it is characterized by the thickness of the boundary layer across which the counter diffusion occurs as shown schematically in Fig. 2 [31]. The solute flux through the membrane is given by the product of the permeate volume flux J_v and the permeate solute concentration C_{A3}. In the boundary layer this net solute flux is also equal to the convective solute flux towards the membrane $J_v C_A$ minus the diffusive solute flux away from the membrane, expressed by Fick's law. From simple mass balance, transport of solute at any point within the boundary layer can be described by the well-known film theory relation [32], Eq. (1). An alternative form of Eq. (1) replaces the concentration terms by observed enrichment factor E_o, defined as C_{A3}/C_{A1} and true enrichment factor E, defined as C_{A3}/C_{A2}, and can be written as [31]

$$\left(\frac{1/E - 1}{1/E_o - 1}\right) = \exp\left(\frac{J_v}{k}\right) \quad (21)$$

The increase or decrease of the solute concentration at the membrane surface, compared to the bulk solution concentration, determines the extent of concentration polarization. The ratio of the two concentrations, C_{A2}/C_{A1}, is called the concentration polarization modulus and is a useful measure of the extent of concentration polarization. When the modulus is 1.0, it can be said that no concentration polarization occurs, but as the modulus deviates farther from 1.0, the effect of concentration polarization on membrane selectivity and flux becomes important. From the definitions of E_o and E, the concentration polarization modulus is equal to E_o/E and, from Eqs. (1) and (21), it can be written as [31]:

$$\frac{E_o}{E} = \frac{C_{A2}}{C_{A1}} = \frac{\exp(J_v/k)}{1 + E_o[\exp(J_v/k) - 1]} \quad (22)$$

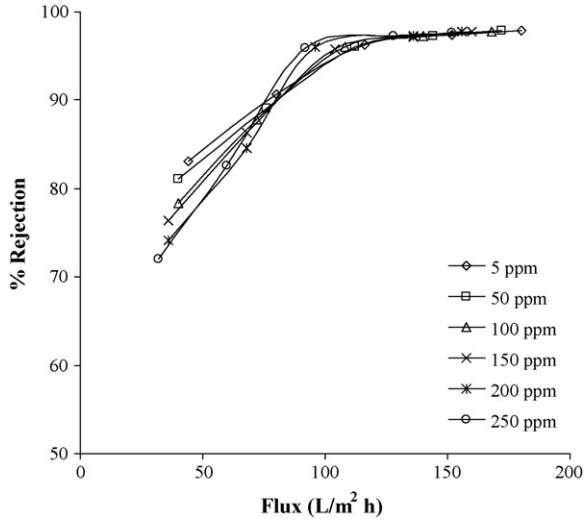

Fig. 3. Flux vs. rejection for different feed solute concentrations (feed rate = 15 L/min).

4. Results and discussion

4.1. Membrane permeability

Before the solute rejection experiments, the PWP of the membrane using distilled water is measured at 30 ± 1 °C. A plot of PWP vs. pressure will give a slope L_P, known as the PWP coefficient of the membrane. The L_P is found to be 13.29 L/(h m^2 atm), which is a typical value of nanofiltration membranes [6,33]. The L_P is considered to be a reference to evaluate cleaning procedure, concentration polarization and fouling of the membrane.

4.2. Effect of applied pressure and feed concentration

Experiments are carried out to study the effect of applied pressure ranging from 4 to 20 atm at fixed pH 3. As shown in Fig. 3, percentage rejections of nickel ions increase slightly with increase in permeate flux for different feed concentrations (5–250 ppm). It is worthwhile mentioning that a high flux with high rejection was obtained at low salt concentration, while the flux and rejection were relatively low at high concentration [23]. Fig. 4 shows the effect of applied pressure on the permeate flux for different feed concentrations. The permeate flux increases linearly with increasing applied pressure, which suggests that there may be negligible concentration polarization in the membrane cell. As the feed concentration increases, the permeate flux decreases due to the increase of concentration difference between the two sides of the NF membrane and subsequent increase in the osmotic pressure that opposes the permeate flow [3,34].

The effect of applied pressure on nickel ions rejection is reported in Fig. 5. It can be seen from Fig. 5 that the rejection increases with increase in applied pressure till 12 atm, because the ion transport due to convection becomes significant compared to diffusion, and thereafter the increase in rejection is negligible reaching a limiting value at 20 atm. The maximum rejection of nickel ions by NF is found to be 98% and 92% for 5 and 250 ppm feed concentration, respectively. In the case of NF, limiting value of rejection depends on the nature of the co-ion (SO_4^{2-}). As a result, salts with SO_4^{2-} ion

Table 1
Parameter estimated using data-fitting method for various models for nickel salt

Set no.	Feed conc. (ppm)	Feed rate (L/min)	CFSD model[a]		CFSK model[b]			CFFP model[c]	
			$D_{AM}K/\delta \times 10^4$	$k \times 10^3$ (cm/s)	σ	$P_M \times 10^5$ (cm/s)	$k^d \times 10^3$ (cm/s)	ε/K	$\varepsilon D_{AB}/\tau\delta \times 10^4$
1	5	5	2.50	4.35	0.9145	5.03	19.23	11.70	5.60
2	5	10	2.45	4.34	0.9107	5.33	20.20	11.20	9.30
3	5	15	2.49	4.39	0.9099	5.60	20.62	11.90	9.30
4	50	5	2.47	4.32	0.9056	5.94	19.05	10.59	9.20
5	50	10	2.48	4.25	0.9052	6.02	20.20	10.55	9.30
6	50	15	2.51	4.15	0.9047	6.14	20.41	10.50	9.20
7	100	5	2.54	4.30	0.9043	6.25	18.87	10.45	9.20
8	100	10	2.53	4.10	0.9020	6.49	19.42	10.50	9.30
9	100	15	2.49	4.05	0.9000	6.71	20.20	10.40	8.70
10	150	5	2.45	3.95	0.8969	6.98	18.69	10.15	9.30
11	150	10	2.43	4.15	0.8947	7.19	19.60	10.35	9.30
12	150	15	2.39	4.14	0.8919	7.40	19.60	10.25	9.30
13	200	5	2.35	4.18	0.8889	7.64	18.52	9.95	9.30
14	200	10	1.75	4.16	0.8863	7.84	19.80	10.05	9.30
15	200	15	2.34	3.97	0.8844	7.98	19.80	9.80	9.30
16	250	5	2.33	4.15	0.8823	8.14	18.35	8.56	10.0
17	250	10	2.38	4.16	0.8802	8.30	19.42	9.88	9.80
18	250	15	2.39	4.25	0.8780	8.47	19.37	8.35	9.50

[a] CFSD is combined-film theory-solution-diffusion model.
[b] CFSK is combined-film theory-Spiegler–Kedem model.
[c] CFFP is combined-film theory-finely porous model.
[d] Mass transfer coefficient value of CFSK model and CFFP model.

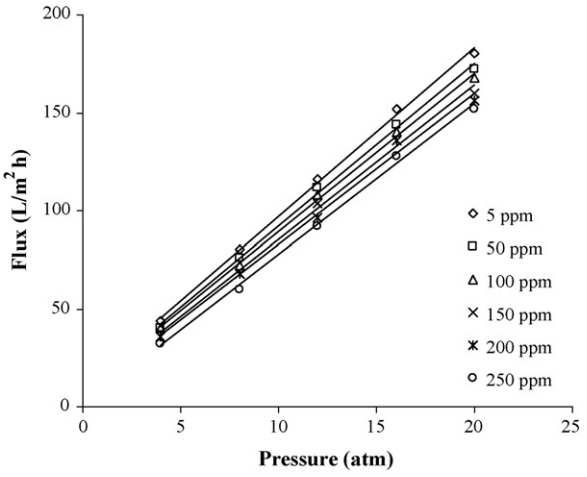

Fig. 4. Influence of applied pressure on the permeate flux for different feed solute concentrations (feed rate = 15 L/min).

Table 2
Comparison of experimental and calculated k values for nickel sulfate–water system

Set no.	$k_{exp} \times 10^3$ (Eq. (16))	$k_{cal} \times 10^3$ (Eq. (25))	Error in k (%)
1	19.29	19.23	0.31
2	20.33	20.20	0.64
3	20.75	20.62	0.63
4	19.06	19.05	0.05
5	20.29	20.20	0.44
6	20.38	20.41	−0.15
7	18.92	18.87	0.26
8	19.98	19.42	2.80
9	20.18	20.20	−0.09
10	18.63	18.69	−0.32
11	19.77	19.60	0.86
12	19.88	19.60	1.41
13	18.48	18.52	−0.22
14	19.72	19.80	−0.41
15	19.72	19.80	−0.41
16	18.24	18.35	−0.60
17	19.40	19.42	−0.10
18	19.34	19.37	−0.15

were rejected more than salts with the Cl^- ion [3,4]. It is observed that the rejection of nickel ions decrease when the concentration increases. This is common for NF membranes [34]. The increase in the feed solution concentration involves a screen formation of cations adjacent to the membrane on high-pressure side. This formation neutralizes the negative charges of the membrane. The total charge of the membrane decreases and the repulsion between the membrane and anion is reduced. As a result, the co-ion will easily pass through the membrane and due to electro-neutrality, the counter-ion will also be rejected less [4]. The same is also true with RO/NF/UF membranes [32–37].

4.3. Effect of feed flowrate

Fig. 6 shows the rejection percentages with change in applied pressures at different feed flowrates (5–15 L/min) for 250 ppm feed concentration. It can be seen from Fig. 6 that the increase in feed flowrate leads to an increase in the solute rejection. The main aim of increasing the feed flow rate is to increase the k, which in turn increases the solute rejection. Similar results are found for the nickel ion [3] and for the zinc ion [37].

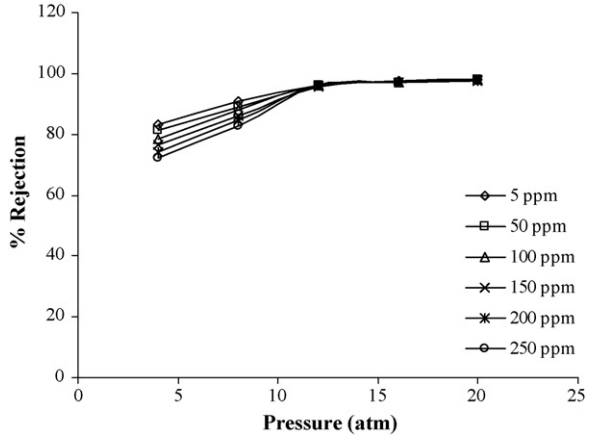

Fig. 5. Influence of applied pressure on the rejection of solute for different solute feed concentrations (feed rate = 15 L/min).

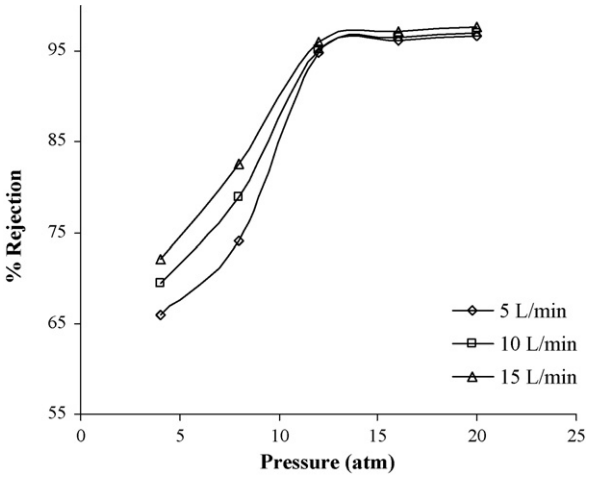

Fig. 6. Influence of applied pressure on the rejection of solute at different feed flow rates (feed concentration = 250 ppm).

4.4. Effect of pH

Fig. 7 shows the effect of pH on the rejection of nickel ions and the permeate flux. The pH is adjusted by the addition of HCl and/or NaOH, depending upon the need. The feed concentration, applied pressure and feed flowrate are fixed at 5 ppm, 15 atm and 15 L/min, respectively. It can be seen from Fig. 7 that there is no significant change in the rejection of nickel ions with respect to change in feed solution pH, and this trend is in line with the results observed by other researchers for the same solute [3,4,38]. The pH variation is having more effect on permeate flux, and the permeate flux reduced considerably with increase in feed solution pH. According to Freger et al. [39] the decrease of membrane permeability at higher pH is due to shrinking of the skin layer due to differences of hydration of ionized groups of the membrane.

4.5. Membrane transport parameters and mass transfer coefficient estimation

The data supplied to the nonlinear parameter estimation program, based on the Levenberg–Marquardt method [40], are R_o and J_v taken at different operating pressures keeping feed rate and feed

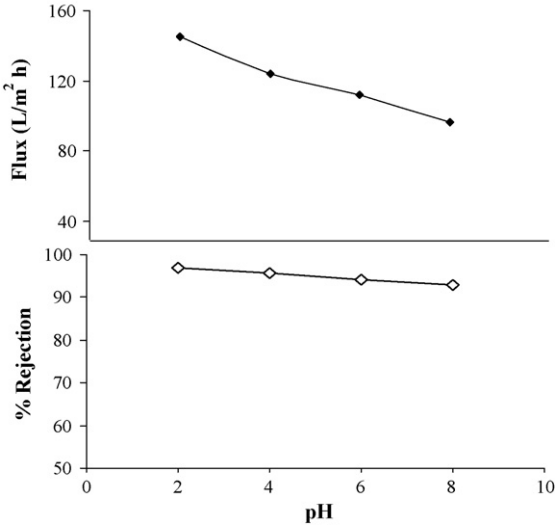

Fig. 7. Influence of pH on the rejection of solute and permeate flux (feed rate = 15 L/min; feed concentration = 5 ppm; applied pressure = 15 atm).

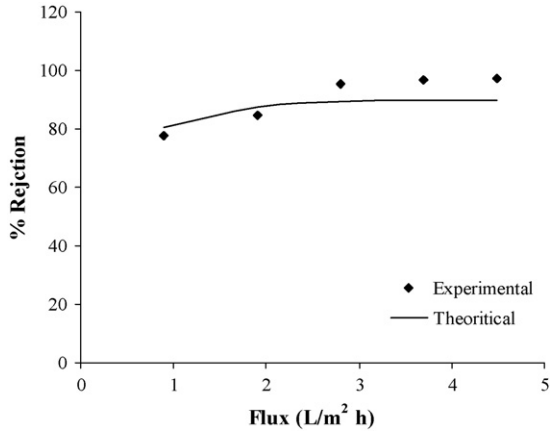

Fig. 8. Results for combined-film theory-solution-diffusion model for 14th set of data for nickel sulphate–water system.

concentration constant for each set of data. The parameters estimated for various models from Eqs. (9), (16) and (18) are used to find the membrane transport parameters and mass transfer coefficients from the respective relations. These parameters are in turn used to calculate observed rejection (R_o) of the membrane for different values of permeate flux (J_v), with respect to the individual model. Sample graphical comparison is also made through Figs. 8 and 9, showing that all the sets are equally fitting. It can be seen from the Figs. 8 and 9 that the model predictions for the rejection values are in good agreement with the experimental results.

The membrane parameters estimated from Eqs. (9), (16) and (18) are given in Table 1. It can be seen that the values of solute permeability P_M and reflection coefficient σ are dependent on the feed concentration. P_M increases with feed concentration due to the high amount of solute passing through the membrane, while σ slightly decreases due to the reduction in solute rejection. The same trend for NF membranes was observed by Al-Zoubi et al. [23]. Ballet et al. [6] and Mehiguene et al [33] investigated the effect of the nature of co-ion on the solute rejection, and found that the reflection coefficient σ for each solute increases with co-ion valency, while the solute permeability P_M decreases with co-ion valency. Similar results were found in literature [6,33,41]. The k values estimated from both the models are used to obtain a simpler relation shown below

$$k \alpha Q^n \tag{23}$$

here, $n = 0.5963$ for CFSK model, and 0.2877 for CFSD model. The mass transfer coefficient is a function of feed flowrate, cell geome-

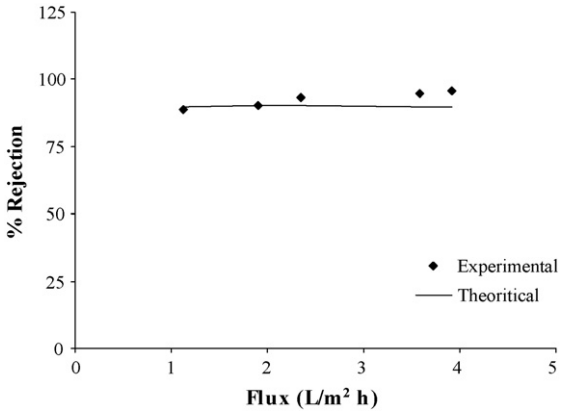

Fig. 9. Results for combined-film theory-Spiegler–Kedem model for 2nd set of data for nickel sulphate–water system.

Table 3
Summary of the enrichment factors (E_o and E), concentration polarization modulus (C_{A2}/C_{A1}) and D_{AB}/l for NF-300 membrane of nickel sulphate–water system at different concentrations and feed flow rates (applied pressure 4 atm)

Set No.	Feed Concentration (ppm)	Feed Flow rate (L/min)	Enrichment factors		Concentration polarization modulus (C_{A2}/C_{A1})	$k \times 10^3$ (cm/s)	Permeate flux $\times 10^3$ (cm/s)	Peclet number (J_v/k)
			E_o	E				
1	5	5	0.1725	0.1655	1.0419	19.23	0.952	0.0495
2	5	10	0.1815	0.1734	1.0466	20.20	1.120	0.0554
3	5	15	0.1695	0.1612	1.0511	20.62	1.232	0.0597
4	50	5	0.2063	0.1987	1.0382	19.05	0.896	0.0470
5	50	10	0.1961	0.1875	1.0458	20.20	1.120	0.0554
6	50	15	0.1889	0.1806	1.0458	20.41	1.120	0.0549
7	100	5	0.2165	0.2081	1.0405	18.87	0.952	0.0505
8	100	10	0.2042	0.1950	1.0472	19.42	1.120	0.0577
9	100	15	0.1932	0.1847	1.0460	20.20	1.120	0.0554
10	150	5	0.2335	0.2256	1.0352	18.69	0.840	0.0449
11	150	10	0.2275	0.2196	1.0361	19.60	0.896	0.0457
12	150	15	0.2164	0.2078	1.0414	19.60	1.008	0.0514
13	200	5	0.2442	0.2365	1.0327	18.52	0.784	0.0423
14	200	10	0.2255	0.2177	1.0359	19.80	0.896	0.0453
15	200	15	0.2288	0.2199	1.0403	19.80	1.008	0.0509
16	250	5	0.2562	0.2481	1.0325	18.35	0.784	0.0427
17	250	10	0.2514	0.2428	1.0353	19.42	0.896	0.0461
18	250	15	0.2498	0.2412	1.0355	19.37	0.896	0.0463

try and solute system. Generalized correlations of mass transfer, in the form of Dittus–Boelter type relation, which have been used by several authors [25,30,42], suggest that the Sherwood number, *Sh*, is related to the Reynolds number, *Re*, and Schmidt number, *Sc*, as

$$Sh = a\,Sc^b Re^c \tag{24}$$

where *a*, *b* and *c* are parameters that need to be determined experimentally. The Leveque's equation [42] is used to evaluate the mass transfer coefficient for flow through thin-channel in laminar flow,

$$k = 0.816\left(\frac{6UD_{AB}^2}{b_c L}\right)^{0.33} \tag{25}$$

The *k* values estimated from CFSK model, Eq. (16), and the Leveque's relation, Eq. (25), for 18 sets of data are shown in Table 2. It can be seen from Table 2 that the maximum deviation observed between the experimental and calculated *k* values is less than 3%. The *k* values estimated using CFSK model are more realistic than those from CFSD model [25,30] and in the present case too the same is observed. Henceforth, these *k* values are used for further calculations.

The effective membrane thickness ($\tau\delta/\varepsilon$) can be calculated from the average value of parameter b_2, and it is found to be 255 μm. If the tortuosity (τ) and the void fraction of the membrane are assumed to be 3 and 0.16, respectively [29], then the membrane active skin layer thickness (δ) will be 14 μm, which is a reasonable value with respect to the data provided by the supplier.

4.6. Estimation of enrichment factors and concentration polarization modulus

Concentration polarization must be incorporated into an RO/NF/UF membrane model in order to determine the true rejection of the membrane that is based on the concentration at the membrane surface in contrast to the observed rejection that is based on the feed concentration. It can be seen from Table 3 that the enrichment factors (E_o and E) for NF-300 membrane are less than 0.16. In the case of reverse osmosis, the enrichment factors are typically about 0.01 [31], because the membrane solute rejection capability will be nearly 100%. Depending on the enrichment term of the membrane, the concentration polarization modulus (C_{A2}/C_{A1}) can be estimated by using Eq. (22) and it can be larger or smaller than 1.0. For NF-300 membrane the concentration polarization modulus is found to be in between (see Table 3). It indicates that the concentration of solute at the membrane surface is 1.0325–1.0511 times larger than it would be in the absence of concentration polarization. In the case of RO, the concentration polarization modulus is normally between 1.1 and 1.5 [31].

The balance between convective transport and diffusive transport in the membrane boundary layer is characterized by the term (J_v/k). This dimensionless number represents the ratio of the convective transport J_v and diffusive transport $k(=D_{AB}/l)$ and is commonly called the Peclet number [31]. The comparison between concentration polarization modulus and Peclet number for NF-300 membrane with nickel sulphate–water system at different concentrations and feed flow rates are also shown in Table 3 when applied pressure is 4 atm. When the Peclet number is large ($J_v \gg k$), the convective flux through the membrane cannot easily be balanced by diffusion in the boundary layer, and the concentration polarization modulus will be large. When the Peclet number is small ($J_v \ll k$), convection is easily balanced by diffusion in the boundary layer, and the concentration polarization modulus is close to unity [31], and this trend is observed in the present case and the Peclet number is between 0.04 and 0.06 when applied pressure is 4 atm, and the maximum being between 0.2 and 0.5 at applied pressure is 20 atm (not shown in Table 3).

5. Conclusions

In the present work performance of NF-300 membrane has been studied to separate nickel ions from dilute wastewaters at different operating conditions. It is observed that the rejection of nickel ions increase with increase in feed pressure and decreases with increase in feed concentration at constant feed flowrates. The maximum rejection of the metal is found to be 98% and 92% for an initial feed concentration of 5 and 250 ppm, respectively. Since the mass transfer coefficient increases with increase in feed flowrate, which in turn reduces the concentration polarization, the rejection increases as the feed flowrate increases at constant feed pressure. The pH effect on the rejection and flux are studied and found that the variation in pH is having not much effect on rejection, where as the flux

decreases with the increase in pH of feed solutions. The membrane transport models; combined-film theory-Spiegler–Kedem (CFSK), combined-film theory-solution-diffusion (CFSD) and combined-film theory-finely porous (CFFP) models; have been used fit the experimental data. CFSK model showed that there is good agreement between the theoretical and experimental rejection data with maximum deviation being less than 10%. The k values calculated from CFSK model are nearer to that of real values with maximum deviation being less than 3%. The CFFP model predicted the effective membrane thickness and the active skin layer thickness, which are in line with data provided by the supplier. The enrichment factors and the concentration polarization modulus have been found for the system and interpreted with the experimental data. The Peclet number found from the data has shown that the mechanism of separation is due to the diffusion.

Acknowledgements

The first author (ZVPM) acknowledges the financial support from the Ministry of Human Resources Development, Government of India, New Delhi, India, under the TAPTEC Research grant (no. F.27-1/2002. TS.V). Thanks are due to Mr. V.Y. Jose, Director, Permionics Limited, Vadodara, India, for providing the Perma-TFC-NF-300 membranes.

References

[1] A.G. Fane, Membranes for water production and wastewater reuse, Desalination 106 (1996) 1–9.
[2] A.G. Fane, A. Yeo, A. Law, K. Parameshwaran, F. Wicaksana, V. Chen, Low pressure membrane processes—doing more with less energy, Desalination 185 (2005) 159–165.
[3] K.H. Ahn, K.G. Song, H.Y. Cha, I.T. Yeom, Removal of ions in nickel electroplating rinse water using low-pressure nanofiltration, Desalination 122 (1999) 77–84.
[4] A.W. Mohammad, R. Othaman, N. Hilal, Potential use of nanofiltration membranes in treatment of industrial wastewater from Ni–P electroless plating, Desalination 168 (2004) 241–252.
[5] M. Nystrom, Separation of metal sulfates and nitrates from their acids using nanofiltration, Membr. Technol. 117 (2000) 5–9.
[6] G.T. Ballet, L. Gzara, A. Hafiane, M. Dhahbi, Transport coefficients and cadmium salt rejection in nanofiltration membrane, Desalination 167 (2004) 369–376.
[7] Y. Garba, S. Taha, J. Cabon, G. Dorange, Modeling of cadmium salts rejection through a nanofiltration membrane: relationships between solute concentration and transport parameters, J. Membr. Sci. 211 (2003) 51–58.
[8] M.T. Ahmed, S. Tahab, R. Maachi, G. Dorange, The influence of physico-chemistry on the retention of chromium ions during nanofiltration, Desalination 145 (2002) 103–108.
[9] H.A. Qdais, H. Moussa, Removal of heavy metals from wastewater by membrane processes: a comparative study, Desalination 164 (2004) 105–110.
[10] Y. Ku, S.W. Chen, W.Y. Wang, Effect of solution composition on the removal of copper ions by nanofiltration, Sep. Purif. Technol. 43 (2005) 135–142.
[11] J. Tanninen, M. Manttari, M. Nystrom, Nanofiltration of concentrated acidic copper sulphate solutions, Desalination 189 (2006) 92–96.
[12] H. Saitua, M. Campderros, S. Cerutti, A.P. Padilla, Effect of operating conditions in removal of arsenic from water by nanofiltration membrane, Desalination 172 (2005) 173–180.
[13] P. Banerjee, S. DasGupta, S. De, Removal of dye from aqueous solution using a combination of advanced oxidation process and nanofiltration, J. Hazard. Mater. 140 (2007) 95–103.
[14] A. Lhassani, M. Rumeau, D. Benjelloun, M. Pontie, Selective demineralization of water by nanofiltration: application to the defluorination of brackish water, Water Res. 35 (2001) 3260–3264.
[15] M. Pontie, C. Diawara, M. Rumeau, D. Aureau, P. Hemmery, Seawater nanofiltration (NF): fiction or reality? Desalination 158 (2003) 277–280.
[16] M.R. Teixeira, M.J. Rosa, M. Nystrom, The role of membrane charge on nanofiltration performance, J. Membr. Sci. 265 (2005) 160–166.
[17] U.B. Cuartas, V.M.C. Vincent, B.S. Alvarez, M.M.I. Alcaina, C.E. Soriano, Nanofiltration of sweet whey and prediction of lactose retention as a function of permeate flux using the Kedem–Spiegler and Donnan Steric Partioning models, Sep. Purif. Technol. 56 (2007) 38–46.
[18] A.L. Ahmad, B.S. Ooi, Properties performance of thin film composites membrane: study on trimesoyl chloride content and polymerization time, J. Membr. Sci. 255 (2005) 67–77.
[19] J. Straatsma, G. Bargeman, H.C. van der Horst, J.A. Wesselingh, Can nanofiltration be fully predicted by a model? J. Membr. Sci. 198 (2002) 273–284.
[20] W. Bowen, M. Jones, J. Welfoot, H. Yousef, Predicting salt rejections at nanofiltration membranes using artificial neural networks, Desalination 129 (2000) 147–162.
[21] O. Kedem, K. Spiegler, Thermodynamics of hyperfiltration (reverse osmosis): criteria for efficient membranes, Desalination 1 (1966) 311–326.
[22] W. Pusch, Determination of transport parameters of synthetic membranes by hyperfiltration experiments. Part I. Derivation of transport relationship from linear relations of thermodynamics of irreversible processes, Ber. Bunsen. Phys. Chem. 81 (1977) 269–276.
[23] H. Al-Zoubi, N. Hilal, N.A. Darwish, A.W. Mohammad, Rejection and modelling of sulphate and potassium salts by nanofiltration membranes: neural network and Spiegler–Kedem model, Desalination 206 (2007) 42–60.
[24] S. Koter, Determination of the parameters of the Spiegler–Kedem–Katchalsky model for nanofiltration of single electrolyte solutions, Desalination 198 (2006) 335–345.
[25] Z.V.P. Murthy, S.K. Gupta, Estimation of mass transfer coefficient using a combined nonlinear membrane transport and film theory model, Desalination 109 (1997) 39–49.
[26] L.S. Clesceri, A.E. Greenberg, A.D. Eaton, Standard Methods for the Examination of Water and Wastewater, 20th ed., American Public Health Association, American Water Work Association, and Water Environment Federation, Washington, DC, 1998.
[27] J.G. Wijmans, R.W. Baker, The solution-diffusion model: a review, J. Membr. Sci. 107 (1995) 1–21.
[28] E.A. Mason, H.K. Lonsdale, Review statistical–mechanical theory of membrane transport, J. Membr. Sci. 51 (1990) 1–81.
[29] M. Soltanieh, W.N. Gill, Review of reverse osmosis membranes and transport models, Chem. Eng. Commun. 12 (1981) 279–363.
[30] S.Y. Vaidya, A.V. Simaria, Z.V.P. Murthy, Reverse osmosis transport models evaluation: a new approach, Indian J. Chem. Technol. 8 (2001) 335–343.
[31] R.W. Baker, Membrane Technology and Applications, 2nd ed., John Wiley & Sons Inc., NJ, 2004.
[32] V.K. Gupta, S.T. Hwang, W.B. Krantz, A.R. Greenberg, Characterization of nanofiltration and reverse osmosis membrane performance for aqueous salt solutions using irreversible thermodynamics, Desalination 208 (2007) 1–18.
[33] K. Mehiguene, Y. Garba, S. Taha, N. Gondrexon, G. Dorange, Influence of operating conditions on the retention of copper and cadmium in aqueous solutions by nanofiltration: experimental results and modeling, Sep. Purif. Technol. 15 (1999) 181–187.
[34] M.D. Afonso, Surface charge on loose nanofiltration membranes, Desalination 191 (2006) 262–272.
[35] Z.V.P. Murthy, S.K. Gupta, Simple graphical method to estimate membrane transport parameters and mass transfer coefficient in a membrane cell, Sep. Sci. Technol. 31 (1996) 77–94.
[36] Z.V.P. Murthy, S.K. Gupta, Sodium cyanide separation and parameters estimation for reverse osmosis thinfilm composite polyamide membrane, J. Membr. Sci. 154 (1999) 89–103.
[37] N. Frares, S. Taha, G. Dorange, Influence of the operating conditions on the elimination of zinc ions by nanofiltration, Desalination 185 (2005) 245–253.
[38] S. Bandini, J. Drei, D. Vezzani, The role of pH and concentration on the ion rejection in polyamide nanofiltration membranes, J. Membr. Sci. 264 (2005) 65–74.
[39] V. Freger, T.C. Arnot, J.A. Howell, Separation of concentrated organic/inorganic salt mixtures by nanofiltration, J. Membr. Sci. 178 (2000) 185–193.
[40] M.S. Bazaraa, H.D. Sherali, C.M. Shetty, Nonlinear Programming Theory and Algorithms, 2nd ed., John Wiley & Sons, NY, 1993.
[41] X.L. Wang, T. Tsuru, M. Togoh, S.I. Nakao, S. Kimura, Transport of organic electrolytes with electrostatic and steric-hindrance effects through nanofiltration membranes, J. Chem. Eng. Jpn. 28 (1995) 372–380.
[42] M.C. Porter, Membrane filtration, in: P.A. Schweitzer (Ed.), Handbook of Separation Techniques for Chemical Engineers, 3rd ed., McGraw-Hill, NY, 1997, pp 2–3 to 2–101.